# THE ROLE OF MESOSCALE STRUCTURES OF THE SOLAR WIND IN THE DEVELOPMENT OF TURBULENCE BEHIND THE BOW SHOCK

**©2025 L.S. Rakhmanova*, M.O. Ryazantseva**, A.A. Khokhlachev***, Yu.I. Yermolaev****,**

**G.N. Zastenker*****

*Space Research Institute of the Russian Academy of Sciences (IKI RAS), Moscow, Russia*

**e-mail: rakhlud@gmail.com*

***e-mail: orearm@gmail.com*

****e-mail: aleks.xaa@yandex.ru*

*****e-mail: yermol@iki.rssi.ru*

******e-mail: gzastenk@iki.rssi.ru*

Received March, 08 2024

Revised May, 16 2024

Accepted for publication July, 25 2024

**Abstract.** This work evaluates the contribution of mesoscale structures – variations registered by satellites over a time period of about 10 minutes – to the development of turbulence in the transition region behind the Earth's bow shock. The study is based on simultaneous measurements of plasma parameters and/or magnetic field in the solar wind, in the dayside magnetosheath, and on the flanks. Data from the Wind, THEMIS, and Spektr-R satellites are used. The characteristics of fluctuation spectra of the magnetic field magnitude and ion flux in the frequency range of $0.01 - 4$ Hz, where the transition from MHD to kinetic scales is observed, are analyzed. It is shown that the dynamics of turbulence characteristics in the transition region is determined by large-scale disturbances, while in their absence, smaller-scale structures can influence the formation of the turbulent cascade.

**Keywords:** *solar wind, magnetosheath, plasma, turbulence, space weather*

**DOI:** 10.31857/S00167940250104e9

# 1. INTRODUCTION

The interaction of the solar wind (SW) and the Earth's magnetosphere is a complex process, in which the transition region behind the Earth's bow shock (EBS) - the magnetosheath (MSH) - plays an important role. Models of the magnetosphere's response to interplanetary disturbances use measurements in the SW as input parameters; however, the properties of plasma and magnetic field in front of the magnetopause, including the characteristics of their variations, can differ significantly from the undisturbed SW. As a number of studies show, in the MSH there is a modification of plasma and magnetic structures coming from the SW [Rakhmanova et al., 2016]; [Turc et al., 2017]. In particular, directly in front of the magnetopause, some of the most geoeffective parameters - the sign and magnitude of the *Bz component* of the magnetic field - may differ from those observed in the SW [Turc et al., 2017]; [Pulinets et al., 2014]; [Šafránková et al., 2009].

It is well known that large-scale disturbances in the solar wind, such as interplanetary coronal mass ejections (ICME) and compression regions ahead of high-speed streams from coronal holes (CIR) are the most geoeffective events [Yermolaev et al., 2012]. Enhanced influence on the magnetosphere is typically due to the presence of prolonged periods of southward orientation of the interplanetary magnetic field ( $Bz < 0$) in such structures, as well as increased dynamic pressure or energy flux (Poynting vector) in such events [Yermolaev et al., 2012]. However, detailed analysis shows that the internal structure of large-scale SW disturbances may also be significant. For example, a compression region may be present ahead of an ICME, preceded by a shock wave, and such ICMEs have different geoeffectiveness [Yermolaev et al., 2012]. Various discontinuities also form within the compression region, each of which can cause a magnetospheric response [Blum et al., 2021]. Various disturbances in the SW are accompanied by peculiarities in processes downstream of the bow shock, in particular, the interaction of the compression region with the magnetosphere is characterized by increased generation of jets (structures with dimensions on the order of Earth's radius, characterized by a sharp increase in plasma density) in the magnetosheath [LaMoury et al., 2020], which exert additional impact on the magnetopause [Dmitriev et al., 2021]. The internal structure of ICMEs also has its own dynamics, and crossing the bow shock affects this dynamics. As shown in the work [Turc et al., 2017], when crossing the bow shock inside magnetic clouds, the sign of the *Bz*

component of the magnetic field can change to the opposite on time intervals of about 30 minutes. Thus, the geoeffectiveness of large-scale solar wind disturbances (having spatial scales on the order of $10^7$ km) can also be determined by embedded smaller-scale structures (variations with scales on the order of $10^5$ km, registered over periods of about units-tens of minutes, hereinafter referred to as medium-scale structures), as well as their modification in the magnetosheath. Such structures in the SW are typically discontinuities of various types [Tsurutani et al., 2010]. Within the framework of solar-terrestrial relationship analysis, it is important to understand how structures of various scales can change in the magnetosheath and what factors influence this process.

There are several approaches to studying processes occurring in MSL at different scales, for example, analysis of individual structures [Rakhmanova et al., 2016]; [Rakhmanova et al., 2018]; [Turc et al., 2017], analysis of averaged values of parameter variations [Nemecek et al., 2000]; [Shevyrev et al., 2003], analysis of the contribution of various wave modes [Anderson et al., 1996]; [Breuillard et al., 2016]. One approach is to analyze the spectrum of turbulent fluctuations in plasma parameters and magnetic field and the dependence of its characteristics on external factors. This approach allows considering a set of processes in a certain range of scales, as well as the interaction of structures of different scales with each other. Spectra provide insight into the processes responsible for energy transfer in the turbulent cascade. The characteristics of turbulence in the SW [Bruno and Carbone, 2013]; [Alexandrova et al., 2013] have been most comprehensively studied to date. It is believed that at scales larger than $10^6$ km, energy enters the system due to large-scale structures arising in the solar corona, energy is transferred to smaller scales through nonlinear interactions of turbulent vortices, forming the inertial range of the cascade, and at scales of the order of the proton gyroradius (~$10^3$ km), energy dissipation begins and plasma heating occurs. Experimental studies show that at the scales of energy input, the spectrum of magnetic field fluctuations is characterized by a power function $f^{-1}$ [Bruno et al., 2009], when transitioning to the inertial range of the cascade (so-called MHD scales), the spectrum is described by a power function $f^{-5/3}$ (corresponding to the classical Kolmogorov spectrum) [Bruno et al., 2009]; [Smith et al., 2006], and at sub-ion (kinetic) scales, there is a transition to the dissipation range, in which the power exponent lies in the range from -2 to -4 [Alexandrova et al., 2012]; [Smith et al., 2006]. The power exponent is determined by the dissipation processes occurring in the plasma, for example, Landau damping, intermittency, as

well as the presence of plasma and magnetic structures such as thin current sheets or Alfvén vortices. In addition, wave processes influence the characteristics of spectra at kinetic scales [Breuillard et al., 2016].

Plasma and magnetic field turbulence in the MSH has been studied to a lesser extent than in the SW, due to significantly more complex dynamics of processes in this region. Compared to the quiet SW, in the MSH turbulence constantly develops in the presence of boundaries - the bow shock and magnetopause. In addition, processes inside the MSH, including the formation of a turbulent cascade, are significantly influenced by the direction of the interplanetary magnetic field relative to the bow shock: at an angle $\theta_{BN} < 45°$ between the interplanetary magnetic field vector and the local normal to the bow shock (quasi-parallel bow shock), the power of fluctuations in the MSH significantly increases [Shevyrev et al., 2005], while at $\theta_{BN} > 45°$ (quasi-perpendicular bow shock), the power of fluctuations in the MSH is significantly lower (about 10% of the parameter value), but a significant temperature anisotropy is observed, leading to the generation of wave processes [Schwartz et al., 1996]. As experimental studies show, downstream of the bow shock, the spectrum of fluctuations at MHD scales differs significantly from the Kolmogorov form [Czaykowska et al., 2001]; [Huang et al., 2017]. It is assumed that mixing of fluctuation phases occurs at the bow shock, and as a result, an inertial region of the cascade is not observed in the dayside MSH, while during plasma propagation towards the flanks, a turbulent cascade develops and a classical Kolmogorov spectrum forms [Huang et al., 2017]. However, a number of studies show that such a change is not always observed [Rakhmanova et al., 2019] and depends on the parameters of the incoming SW flow [Rakhmanova et al. 2020, 2022]. In particular, it is shown that during periods of quiet SW flow, the fluctuation spectra in the MSH are close to those observed in the SW, whereas during periods of large-scale disturbances in the interplanetary medium (ICME, CIR), strong changes in turbulence characteristics occur at the bow shock, including the absence of Kolmogorov scaling at MHD scales and steepening of spectra at kinetic scales.

Currently, there is an understanding of turbulence properties in different regions of the MSL [Huang et al., 2017]; [Rakhmanova et al., 2018]; [Rakhmanova et al., 2018]; [Li et al., 2020], obtained based on statistical analysis of measurements across the ESBW. In addition, there are experimental indications of the features of turbulence formation behind the ESBW for various large-scale types of SW [Rakhmanova et al., 2018]; [Rakhmanova et al., 2022]. However,

as shown above, within large-scale interplanetary disturbances, there are always medium-scale structures that are subject to changes at the ESBW. In this case, structures refer to rapid changes in magnetic field parameters (rotation) or plasma, or their variations. Sharp rotations of the magnetic field, accompanied by changes in plasma parameters, are known to be characteristic of such phenomena in the SW as tangential and rotational discontinuities [Tsurutani et al., 2010]. The influence of such structures on the dynamics of the turbulent cascade in the MSL has not yet been investigated, despite the contribution to solar-terrestrial relationships mentioned in the literature [Blum et al., 2021].

In the present work, based on several events, we analyze how medium-scale structures can influence the process of turbulent cascade modification at the ESBW. Events are considered when measurements are available from three satellites – in the SW, in the dayside MSL, and on the MSL flank. Data from the Wind, THEMIS, and Spektr-R satellites are used. In order to assess the difference between quiet and disturbed conditions in the SW, periods of slow undisturbed SW and ICME, including compression regions in front of them, are identified. The characteristics of Fourier spectra of magnetic field magnitude fluctuations and ion flux in the frequency range of 0.01–4 Hz are analyzed.

## 2. DATA

This work used simultaneous measurements from three satellites located in different regions of near-Earth space, taking into account the propagation time of plasma between satellites. Solar wind data were obtained from the Wind satellite: plasma characteristics were measured using the SWE instrument [Ogilvie et al., 1995] with a resolution of 92 s or the 3DP instrument [Lin et al., 1995] with a resolution of 3 s, while the magnitude and components of the magnetic field were measured by the MFI instrument [Lepping et al., 1995] with a time resolution of 0.092 s. In the magnetosheath, measurements from one of the THEMIS mission satellites were used, with plasma parameters measured by the ESA instrument [Auster et al., 2008] with a resolution of 3-4 s, and magnetic field characteristics measured using the FGM instrument [McFadden et al., 2008] with a resolution of 0.25 s.

It should be noted that in the case of the Wind and THEMIS satellites, the high time resolution magnetic field measurements were key in this analysis, while plasma parameters were used as auxiliary data, particularly for tracing plasma between satellites.

Additionally, in the magnetosheath, data from the BMSW instrument [Zastenker et al., 2013]; [Šafránková et al., 2009] on the Spektr-R satellite were used. Measurements of plasma density, velocity, and temperature with a time resolution of 3 s and ion flux measurements with a resolution of 0.031 s were utilized.

Three time intervals from different days were selected: 1) quiet solar wind, 2) compression region before an ICME, 3) ICME together with the compression region preceding it. The main criterion for event selection was the simultaneous availability of measurements with the highest accessible time resolution on all three satellites, as well as an interval duration of at least 2 hours. Events were considered where similar time series of density changes were observed at all three satellites, ensuring that the same plasma was being examined at three points. All selected events pertained to the magnetosheath behind the quasi-perpendicular bow shock.

Fig. 1.

Figure 1 *a* shows plasma density measurements from the Wind (solar wind, dark gray line), Spektr-R (dayside magnetosheath, light gray line), and THEMIS-C (flank, black line) satellites. The left y-axis corresponds to Wind and THEMIS-C measurements, while the right y-axis corresponds to Spektr-R measurements. The positions of the satellites in near-Earth space are shown in panel ( *g* ); the bow shock and magnetopause are shown schematically.

The main problem in analyzing multi-satellite measurements is determining the plasma propagation time between spacecraft. In this work, at the first stage, the shift was calculated as the distance between satellites divided by the SW plasma velocity. Then, plasma and/or magnetic field structures visible on all satellites were manually identified, and the data time series were shifted so that the structures coincided. For the example shown in Fig. 1, the time shift between Wind and Spektr-R was 3590 s, between Spektr-R and THEMIS-C – 1545 s. In Fig. 1 *a* a number of structures can be clearly traced on all three satellites (for example, density increases at ~17:50 UT, ~18:10 UT).

Fig. 2.

In Fig. 2, panels *b, c* show magnetic field measurements from THEMIS-C and Wind, respectively, shifted by the same time as the plasma density time series. Magnetic field measurements from the Spektr-R satellite are not available. It is clearly seen that the same magnetic field structures (e.g., at ~17:50 UT, ~18:45 UT) are observed on the pair of satellites, despite the significant distance between them. A more detailed description, features, and

problems of comparing data from several satellites in the SW and MSL are given in [Rakhamnova et al., 2022].

To analyze the influence of medium-scale structures on turbulence characteristics, intervals were selected from the time series during which these structures were registered on all three satellites, as well as quasi-stationary intervals where structures were not observed. Fig. 1 *a*−*c* highlights three selected intervals. The duration of the intervals was chosen to provide a sufficient number of points for Fourier analysis, and is ~17 min for Spektr-R and THEMIS data and 25 min for Wind data. The difference in interval duration is due to different time resolutions of the analyzed data; while the midpoints of the Wind and THEMIS-C/Spektr-R data intervals coincide. During intervals 1 and 3, field rotations (sharp changes in one of the components) and plasma density changes are observed. During interval 2, plasma and magnetic field on all three satellites are quasi-stationary.

It should be noted that within the framework of this work, medium-scale structures are considered as structures with changes in plasma density accompanied by rotation of the magnetic field. Analysis of the type of these structures is not conducted.

For the intervals selected in the presented manner, Fourier spectra of fluctuations in the magnetic field magnitude (based on Wind and THEMIS data) and ion flux (based on Spektr-R data) were calculated. Variations of both parameters represent compression variations, and their spectra typically have the same scaling [Chen, 2016]; [Chen and Boldyrev, 2017]; [Breuillard et al., 2018]. To compare different parameters with each other, the spectra of magnetic field fluctuations and ion flux were normalized to the mean value of the parameter for the interval.

## 3. RESULTS

The example presented in Fig. 1 refers to the period of slow undisturbed SW (type *Slow* according to the catalog [Yermolaev et al., 2009]). Fig. 2 *a*−*c* shows spectra for three selected intervals, each panel presents three spectra - in the SW (dark gray line, fluctuations of magnetic field magnitude | *B* |), in the dayside part of the MSL (light gray line, fluctuations of ion flux | *F* |) and on the flank of the MSL (black line, fluctuations of magnetic field magnitude | *B* |). Dashed lines represent the results of approximating the spectra with power functions. In this work, Fourier spectra are calculated for different parameters - magnetic field magnitude and ion flux - due to the absence of magnetic field measurements on the Spektr-R satellite. Ion flux fluctuations represent density fluctuations, since the plasma velocity magnitude varies to a lesser extent

(direct comparison of spectra of ion flux fluctuations and plasma density was conducted in [Pitňa et al. 2016]). Fluctuations of plasma density and magnetic field magnitude represent the compression component of the turbulent cascade and typically have similar characteristics. Additionally, identical scaling of magnetic field magnitude and density was shown by simultaneous measurements on one satellite for both MHD [e.g., Chen 2016] and at kinetic scales [Chen and Boldyrev 2017; Breuillard et al. 2018]. Therefore, in this work, it is assumed that comparing the properties of fluctuation spectra of these quantities is justified if only the scaling of fluctuations is considered, not their power.

Interval 1 is characterized by a spectrum of $\sim f^{-1.7\pm0.2}$ in the SW at MHD scales and $f^{-2.7\pm0.1}$ at kinetic scales. At MHD scales, the spectrum is close to the Kolmogorov form, typical for SW plasma. At kinetic scales, the spectral slope also corresponds to average SW values and is close to -8/3, predicted by some theories [Boldyrev and Perez, 2012]. Behind the EOSC, a significant flattening of the spectrum at MHD scales is observed, with a spectral slope of -1±0.3, which is typical for turbulence in the dayside magnetosheath [Czaykowska et al., 2001]; [Huang et al., 2017]. At kinetic scales, the spectrum has a slope of -2.6±0.1, close to -8/3 and to what is observed in the SW. On the flanks, it is impossible to determine the spectral slope at MHD scales due to the presence of a peak at transitional scales caused by wave processes. At kinetic scales, the spectrum has a slope of -2.1±0.3, i.e., the spectrum is flatter than in the SW and in the dayside magnetosheath. Thus, in this event, at the EOSC, there was an expected significant change in the scaling of the turbulent cascade at MHD scales and preservation at kinetic scales, while during propagation to the flanks, a flattening of the kinetic part of the spectrum occurred, which may be due to the enhancement of compression fluctuations.

Similarly, a comparison of turbulence characteristics was conducted for other intervals. As can be seen from Fig. 2 *b* , for interval 2, which lacks medium-scale structures, a slope of -1.8±0.2 is observed in the SW at MHD scales, which is close to Kolmogorov scaling, while the slope at kinetic scales is -2.3±0.1, which is close to -7/3, also often predicted in theories [Schekochihin et al., 2009]. In the dayside magnetosheath, enhanced wave activity leads to the appearance of a broad peak in the spectrum at frequencies of 0.05-0.8 Hz, making it impossible to determine the slope at MHD scales. In the frequency range after the break, the spectral slope is -2.1±0.1, which is observed quite rarely in both the magnetosheath and the SW. Thus, behind the EOSC, a slight flattening of the spectrum at kinetic scales is observed. During propagation to the

flanks, the peak in the spectrum persists, indicating the locality of the wave process responsible for it. At kinetic scales, a restoration of the spectral slope to -2.3±0.2 is observed, close to that observed in the SW.

For interval 3, during which medium-scale structures are registered, in the SW a slope of -1.6±0.1 is observed at MHD scales, i.e., Kolmogorov spectrum, and -2.3±0.1 at kinetic scales. In the dayside MSL at MHD scales, the spectrum flattens to $f^{-1.2\pm0.3}$, while at kinetic scales the spectrum does not change and has a slope of -2.3±0.1. On the flanks of the MSL, at MHD scales, the spectrum is characterized by a slope of -0.8±0.1, i.e., it also differs from the Kolmogorov spectrum. At kinetic scales, the spectral slope is -2.4±0.1, which is close to observations in the SW and in the dayside MSL.

Thus, under quiet SW conditions in the absence of medium-scale structures (interval 2), in the dayside MSL, the main contribution to the spectra of turbulent fluctuations at MHD scales comes from wave processes, which leads to the dominance of a peak in the spectrum at frequencies close to the break. At kinetic scales, the spectra slightly flatten behind the OEBS to power-law indices that are statistically observed quite rarely. When propagating toward the flanks, the peak in the spectrum persists, implying that the source of the wave process moves to the flanks along with the plasma. At kinetic scales, there is a restoration of scaling characteristic of the SW. It should be noted that typically in the MSL, either ion-cyclotron Alfvén instabilities or mirror mode waves, which are compression variations, are observed. It can be assumed that the overall low level of fluctuations leads to the fact that after crossing the OEBS, the main contribution to the development of the turbulent cascade is made by the compressional mirror mode.

In the presence of medium-scale structures (intervals 1, 3) at MHD scales behind the OEBS, the Kolmogorov scaling characteristic of turbulence in the SW disappears, which is generally typical for the dayside MSL [Huang et al., 2017]. At the same time, at kinetic scales, the spectral slope is preserved in the dayside MSL. However, when propagating to the flanks, there is no restoration of Kolmogorov scaling, which typically occurs as plasma moves away from the subsolar region of the MSL [Rakhmanova et al., 2022]. In addition, at kinetic scales, a flattening of the spectra may be observed. It is worth noting that in this case, a peak of compressional fluctuations was also present at the frequencies of the spectral break.

Fig. 3.

Figure 3 (similar to Figure 1) shows an event related to the compression region *Sheath* ahead of the ICME. In the ICME region itself, the necessary measurements were missing. In the dayside MSL, the THEMIS-E satellite (until 00:10 UT) and the THEMIS-A satellite (after 00:10 UT) were located. During the event, 4 intervals can be identified: in intervals 1 and 3, both in the SW and MSL, significant density variations and magnetic field rotations are observed (accompanied by changes in the sign of the *Bz component),* in intervals 2 and 4, despite the presence of variations in all magnetic field components typical for this type of SW, there is no change in the sign of *Bz* , and there are no significant plasma density variations. In this event, intervals 1 and 3 were considered as intervals with medium-scale structures, events 2 and 4 - as quasi-stationary intervals without structures.

Fig. 4.

Similarly, Figure 4 shows the event of February 16, 2014, in which it is possible to conduct analysis for both the *Sheath* region and the ICME (magnetic cloud, MC) before which this region was formed. Intervals 1 and 3 are characterized by the absence of structures, intervals 2 and 4 contain medium-scale structures. As can be seen from Fig. 4, the time shift that ensures the coincidence of structures in the *Sheath* region leads to a divergence of magnetic structures in the MC region (at 05:00-05:30 UT). This occurs due to differences in the propagation speed of various SW structures. In this case, for each of the considered intervals, the shift between the time series data was adjusted separately.

The approximation of the obtained spectra was carried out similarly to the case of quiet SW. The characteristics of the spectra for all considered intervals are given in Table 1.

Table 1.

Table 1 shows the sequence number of the interval, the date of the event, the type of SW and the interval number in the figure, the presence of medium-scale structures within the interval, as well as the values of the spectral slopes in three regions of near-Earth space at both MHD and kinetic scales. In some cases, determining the slope at MHD scales is impossible due to wave processes.

Comparison of the spectral slopes in different locations for disturbed SW shows that at MHD scales, strong wave activity is typically observed in the dayside MSh, which interferes with the determination of scaling. However, intervals 4-7 are characterized by both the preservation of scaling at MHD scales when crossing the LLBL and significant flattening of the spectra, with

flattening possibly observed both against the background of medium-scale structures and without them. Moreover, the spectra beyond the LLBL are characterized by more significant flattening than for quiet SW. Similar changes at the LLBL were previously noted for disturbed SW [Rakhmanova et al., 2022], and are a characteristic change in turbulence properties at the LLBL.

For most events on the flanks, Kolmogorov spectra are observed at MHD scales, which is characteristic of this region. For events 8 and 11, however, the spectra remain flatter than in the SW. These events are observed both against the background of quasi-stationary SW and in the presence of medium-scale structures, i.e., these structures do not influence this process.

At kinetic scales, for most events (except 6, 7), steepening of the spectra is observed beyond the LLBL regardless of the presence of medium-scale structures. The steepest spectra in the dayside MSh (with slopes up to -4.8) are observed during ICME periods, which is in good agreement with previous results [Rakhmanova et al., 2022]. For events 6 and 7, observed during periods of interaction with the MSh compression regions *Sheath* , unusually steep spectra are observed in the SW and their flattening in the dayside MSh. Interestingly, intervals 6 and 7 are characterized by the presence and absence of medium-scale structures, respectively. That is, the processes responsible for changing the spectrum at the LLBL are not related to medium-scale structures in this case either.

On the MSL flanks at kinetic scales, spectra with slopes of –(2.6-3.2), characteristic of MSL turbulence, are typically formed. At the same time, no connection is observed between the slope values in the SW and on the flank and the presence of medium-scale structures. However, peculiarities in the spectra are observed in the events 6 and 7 considered above: they are characterized by flattening of the spectra on the flanks to values of –(2.0-2.2). This property of compression regions ( *Shearh* and CIR) has been noted previously [Rakhmanova et al., 2022], and, as can be seen from the data in Table 1, is not related to the presence of medium-scale structures.

It should be noted that for the events under consideration, during periods of quiet SW on the flank, spectra of ion flux fluctuations were analyzed, while during periods of disturbed SW on the flank, fluctuations of the magnetic field magnitude were considered. However, the spectral slopes obtained for the ion flux are in good agreement with those previously obtained for fluctuations of the magnetic field magnitude in the same region [Rakhmanova et al. 2022] also for quiet SW conditions. In addition, comparison of the spectra of ion flux fluctuations and

magnetic field magnitude on the flank (at different distances toward the magnetospheric tail) from the Spektr-R and THEMIS satellites have the same scaling. Despite the difference in measured parameters, compressible fluctuations demonstrate the same scaling, so it can be concluded that the differences identified in this work for quiet and disturbed SW are due to the peculiarities of the development of the compressible component of the turbulent cascade under different SW conditions, and not due to the difference in the parameters considered.

Thus, during periods of disturbed solar wind, the main changes in the turbulent cascade (such as flattening at MHD scales and significant steepening at kinetic scales) are determined by the large-scale SW type and do not depend on the dynamics of structures within the large-scale disturbance.

## 4. CONCLUSION

Based on the comparison of simultaneous measurements at three points in near-Earth space - in the SW, in the dayside MSL, and on the MSL flank - the paper analyzes how the presence of medium-scale structures (variations recorded by the satellite over time periods of ~10 min) may affect the dynamics of the turbulent cascade behind the EFBS. It is shown that:

1. During periods of undisturbed slow SW in the absence of medium-scale structures, the dynamics of the turbulent cascade in the MSL is determined by wave processes arising behind the EFBS.
2. During periods of undisturbed slow SW in the presence of medium-scale structures behind the EFBS, spectral slopes at MHD scales close to -1 are observed, which may be associated with a violation of the conditions for developed turbulence and the absence of an inertial range in the turbulent cascade; there is no restoration of spectra characteristic of developed turbulence on the MSL flanks.
3. During periods of quiet slow SW, the characteristics of turbulence at kinetic scales do not change when plasma enters the MSL and propagates to the flanks, which indicates the universality of energy dissipation processes before and after the EFBS; in some cases, flattening of spectra may be observed as plasma propagates to the flanks, probably caused by local instabilities.
4. The presence of medium-scale structures against the background of large-scale disturbances in the SW does not affect the modification of turbulence characteristics at the EFBS:

all changes - the absence of Kolmogorov scaling at MHD scales and the steepening of spectra at kinetic scales in the dayside MSL and the restoration of a form close to that observed in the SW on the flanks - correspond to the previously presented statistics both in the presence and absence of medium-scale structures.

Thus, it is shown that the main contribution to the development of the turbulent cascade at the EFBS is made by large-scale disturbances in the solar wind. The dynamics of smaller-scale structures (about 10 minutes) may have an influence on turbulence behind the EFBS against the background of quiet conditions in the solar wind.

FUNDING

The research is supported by the Russian Science Foundation, grant No. 22-12-00227, ( https://rscf.ru/project/22-12-00227/ ).

REFERENCES

– *Yermolaev Yu.I., Nikolaeva N.S., Lodkina I.G., Yermolaev M.Yu.* Catalog of large-scale solar wind phenomena for the period 1976−2000 // Cosmic Research. Vol. 47. No. 2. P. 99–113. 2009.

– *Zastenker G.N., Shafrankova J., Nemechek Z., et al.* Fast measurements of solar wind parameters using the BMSW instrument // Cosmic Research. Vol. 51. No. 2. P. 88–99. 2013.

– *Pulinets M.S., Ryazantseva M.O., Antonova E.E., Kirpichev I.P.* Dependence of magnetic field parameters near the subsolar point of the magnetosphere on the interplanetary magnetic field based on THEMIS experiment data // Geomagnetism and Aeronomy. Vol. 52. No. 6. P. 769–778. 2012.

– *Rakhmanova L.S., M.O. Ryazantseva, G.N. Zastenker, M.I. Verigin, Yu.I. Yermolaev, I.G. Lodkina* Influence of interplanetary medium parameters and magnetosheath boundaries on the correlation coefficient value between ion flux in the solar wind and magnetosheath // Geomagnetism and Aeronomy. Vol. 58. No. 4. P. 463–470. 2018.

– *Rakhmanova L.S., Ryazantseva M.O., Zastenker G.N., Yermolaev Yu.I., Lodkina I.G., Chesalin L.S.* Influence of Solar Wind Plasma Turbulence Characteristics on Turbulent Cascade Properties in the Magnetosheath // Space Research. V. 57. № 6. P. 1–8. 2019.

– *Alexandrova O., Lacombe C., Mangeney A., Grappin R., Maksimovic, M.* Solar wind turbulent spectrum at plasma kinetic scales // Astrophys. J. V. 760. N 2. P. 121–126. 2012. https://doi.org/10.1088/0004-637X/760/2/121

– *Alexandrova O., Chen C. H. K., Sorriso-Valvo L., Horbury T. S., Bale S. D.* Solar Wind Turbulence and the Role of Ion Instabilities // Space Sci. Rev. V. 178. P. 101–139. 2013. https://doi.org/10.1007/s11214-013-0004-8

– *Anderson B.J., Fuselier S.A., Gary S.P., Denton R.E.* Magnetic spectral signatures in the Earth's magnetosheath and plasmadepletion layer // J. Geophys. Res. V. 99. P. 5877–5891. 1994. https://doi.org/10.1029/93JA02827

– *Angelopoulos V.* The THEMIS mission // Space Sci. Rev. V. 141. P. 5–34. 2008. https://doi.org/10.1007/s11214-008-9336-1

– *Auster H. U., Glassmeier K. H., Magnes W., et al.* The THEMIS Fluxgate Magnetometer // Space Sci. Rev. V. 141. N 1–4. P. 235–264. 2008. https://doi.org/10.1007/s11214-008-9365-9

– *Blum L. W., Koval A., Richardson I. G., Wilson L. B., Malaspina D., Greeley A., Jaynes A. N.* Prompt response of the dayside magnetosphere to discrete structures within the sheath region of a coronal mass ejection // Geophysical Research Letters. V. 48. e2021GL092700. 2021. https://doi.org/10.1029/2021GL092700

– *Boldyrev S., Perez J. C.* Spectrum of Kinetic Alfven Turbulence // Astrophys. J. Lett. V. 758. N 2. L44. 2012. https://doi.org/10.1088/2041-8205/758/2/L44

– *Borodkova N., Zastenker G., Riazantseva M., Richardson J.* Large and sharp solar wind dynamic pressure variations as a source of geomagnetic field disturbances at the geosynchronous orbit // Planet. Space Sci. V. 53. P. 25−32. 2005. https://doi.org/10.1016/j.pss.2004.09.025

– *Breuillard H., Matteini L., Argall M. R., et al.* New Insights into the Nature of Turbulence in the Earth's Magnetosheath Using Magnetospheric Multi Scale Mission Data // Astrophys. J. V. 859. 127. 2018. https://doi.org/10.3847/1538-4357/aabae8

– *Breuillard H., Yordanova E., Vaivads A., Alexandrova O.* The effects of kinetic instabilities on small-scale turbulence in Earth's magnetosheath // Astrophys. J. V. 829. 54. 2016. https://doi.org/10.3847/0004-637X/829/1/54

– *Bruno R., Carbone V., Vörös Z., et al.* Coordinated Study on Solar Wind Turbulence During the Venus-Express, ACE and Ulysses Alignment of August 2007 // Earth Moon Planets. V. 104. P. 101–104. 2013. https://doi.org/10.1007/s11038-008-9272-9

Bruno *R., Carbone V.* The Solar Wind as a Turbulence Laboratory // Living Rev. Sol. Phys. V. 10. № 2. 2013. https://doi.org/10.12942/lrsp-2013-2

– *Chen C. H. K.* Recent progress in astrophysical plasma turbulence from solar wind observations. // J. Plasma Phys. V. 82. 535820602. 2016. https://doi.org/10.1017/S0022377816001124

– *Chen C. H. K., Boldyrev S.* Nature of Kinetic Scale Turbulence in the Earth's Magnetosheath // Astrophys. J. V. 842. P. 122–131. 2017. https://doi.org/10.3847/1538-4357/aa74e0

– *Czaykowska A., Bauer T. M., Treumann R. A., and Baumjohann W* . Magnetic field fluctuations across the Earth's bow shock // Ann. Geophys. V. 19. P. 275–287. 2001. https://doi.org/10.5194/angeo-19-275-2001

– *Dmitriev A.V., Lalchand B., Ghosh S.* Mechanisms and Evolution of Geoeffective Large-Scale Plasma Jets in the Magnetosheath // Universe. V. 7. 152. https://doi.org/10.3390/universe7050152

– *Huang S. Y., Hadid L. Z., Sahraoui F., Yuan Z. G., Deng X. H.* On the Existence of the Kolmogorov Inertial Range in the Terrestrial Magnetosheath Turbulence // Astrophys. J. Lett. V. 836. L10. 2017. https://doi.org/10.3847/2041-8213/836/1/L10

– *Lacombe C., Belmont G.* Waves in the Earth's magnetosheath: Observations and interpretations // Adv. Sp. Res. V. 15. P. 329–340. 1995. https://doi.org/10.1016/0273-1177(94)00113-F

– *LaMoury A. T., Hietala H., Plaschke F., Vuorinen L., Eastwood J. P.* Solar wind control of magnetosheath jet formation and propagation to the magnetopause. J. Geophys. Res. Space Phys. // V. 126. N 9. e2021JA029592. 2021. https://doi.org/10.1029/2021ja029592

– *Lepping R. P., Acuna M. H., Burlaga L. F., et al.* The WIND magnetic field investigation // Space Sci. Rev. V. 71. N 1–4. P. 207–229. 1995. https://doi.org/10.1007/BF00751330

– *Li H., Jiang W., Wang C., Verscharen D., Zeng C., Russell C. T., Giles B., Burch J. L.* Evolution of the Earth's Magnetosheath Turbulence: A Statistical Study Based on MMS Observations // Astrophys. J. V. 898. L43. 2020. https://doi.org/10.3847/2041-8213/aba531

– *Lin R. P., Anderson K. A., Ashford S., et al.* Three-Dimensional Plasma and Energetic Particle Investigation for the Wind Spacecraft // Space Sci. Rev. V. 71. P. 125–153. 1995. https://doi.org/10.1007/BF00751328

– *McFadden J.P., Carlson C.W., Larson D., Ludlam M., Abiad R., Elliott B., Turin, P., Marckwordt M., Angelopoulos V.* The THEMIS ESA plasma instrument and in-flight calibration // Space Sci. Rev. V. 141. P. 277–302. 2008. https://doi.org/10.1007/s11214-008-9440-2

– *Němeček Z., Šafránková J., Zastenker G. N., Pišoft P., Paularena K. I., and Richardson J. D.* Observations of the radial magnetosheath profile and a comparison with gasdynamic model 1024 predictions // Geophys. Res. Lett. V. 27. P. 2801–2804. 2000. https://doi.org/10.1029/2000GL000063

– *Ogilvie K. W., Chornay D. J., Fritzenreiter R. J., et al.* SWE, a comprehensive plasma instrument for the Wind spacecraft // Space Sci. Rev.V. 71. N 1–4. P. 55–77. 1995. https://doi.org/10.1007/BF00751326

– *Pitňa A., Šafránková J., Němeček Z., Goncharov O., Němec F., Přech L., Chen C. H. K., Zastenker G.* Density fluctuations upstream and downstream of interplanetary shocks // Astrophys. J. V. 819. 41–50. 2016. https://doi.org/10.3847/0004-637X/819/1/41

– *Rakhmanova L., Riazantseva M., Zastenker G., Yermolaev Y., and Lodkina I.* Dynamics of Plasma Turbulence at Earth's Bow Shock and through the Magnetosheath // Astrophys. J. V. 901. N 30. P. 30–40. 2020. https://doi.org/10.3847/1538-4357/abae00

– *Rakhmanova L., Riazantseva M., Zastenker G. and Yermolaev Y.* Large-Scale Solar Wind Phenomena Affecting the Turbulent Cascade Evolution behind the Quasi-Perpendicular Bow Shock // Universe. V. 8. N 12. P. 611. 2022. https://doi.org/10.3390/universe8120611

– *Rakhmanova L., Riazantseva M., Zastenker G., Verigin M.* Kinetic-Scale Ion Flux Fluctuations Behind the Quasi-Parallel and Quasi-Perpendicular Bow Shock. // J. Geophys. Res. Sp. Phys. V. 123. P. 5300–5314. 2018. https://doi.org/10.1029/2018JA025179

– *Šafránková J., Hayosh M., Gutinska O.,Němeček Z., Přech L.* Reliability of prediction of the magnetosheath Bz component from the interplanetary magnetic field observations // J. Geophys. Res. V. 114. A12213. 2009. https://doi.org/10.1029/2009JA014552

– *Šafránková, J., Němeček, Z., Přech, L., et al.* Fast solar wind monitor (BMSW): description and first results // Space Sci. Rev. V. 175. P. 165–182. 2013. https://doi.org/10.1007/s11214-013-9979-4

– *Schekochihin A. A., Cowley S. C., Dorland W., Hammett G. W., Howes G. G., Quataert E., Tatsuno T.* Astrophysical gyrokinetics: kinetic and fluid turbulent cascades in magnetized

weakly collisional plasmas // Astrophys. J. Suppl. Ser. V. 182. P. 310–377. 2009. https://doi.org/10.1088/0067-0049/182/1/310

– *Schwartz S. J., Burgess D., Moses J. J.* Low-frequency waves in the Earth's magnetosheath: present status // Ann. Geophys. V. 14. P. 1134–1150. 1996. https://doi.org/10.1007/s00585-996-1134-z

– *Shevyrev N. N., Zastenker G. N., Nozdrachev M. N., Němeček Z., Šafránková J., and Richardson J. D.* High and low frequency large amplitude variations of plasma and magnetic field in the magnetosheath: radial profile and some features // Adv. Space Res. V. 31. P. 1389–1394. 2003. https://doi.org/10.1016/S0273-1177(03)00008-5

– *Shevyrev N.N., Zastenker G. N.* Some features of the plasma flow in the magnetosheath behind quasi-parallel and quasi-perpendicular bow shocks // Planet. Space Sci. V. 53. P. 95–102. 2005. https://doi.org/10.1016/j.pss.2004.09.033

– *Smith C., Hamilton K., Vasquez B, Leamon R.* Dependence of the dissipation range spectrum of interplanetary magnetic fluctuations on the rate of energy cascade // Astrophys. J. V. 645: L85–L88. 2006. https://doi.org/10.1086/506151

– *Tsurutani B. T., Lakhina G. S., Verkhoglyadova O. P., Gonzalez W. D., Echer E., Guarnieri F. L.* A review of interplanetary discontinuities and their geomagnetic effects // Journal of Atmospheric and Solar-Terrestrial Physics. V. 73. N 1. P. 5–19. 2011. https://doi.org/ 10.1016/j.jastp.2010.04.001

– *Turc L., Fontaine D., Escoubet C. P., Kilpua E. K. J., Dimmock A. P.* Statistical study of the alteration of the magnetic structureof magnetic clouds in the Earth's magnetosheath // J J. Geophys. Res. Sp. Phys. V. 122. N 3. P. 2956–2972. 2017. https://doi.org/10.1002/2016JA023654

– *Verigin M. I., Tátrallyay M., Erdős G., Kotova G.A* . Magnetosheath – Interplanetary medium reference frame: Application for a statistical study of mirror type waves in the terrestrial plasma environment // Adv. Space Res. V. 37. P. 515-521. 2006. https://doi.org/10.1016/j.asr.2005.03.042

– *Yermolaev Y. I., Nikolaeva N. S., Lodkina I. G., Yermolaev M. Y.* Geoeffectiveness and efficiency of CIR, sheath, and ICME in generation of magnetic storms // J. Geophys. Res. V. 117. A00L07. 2012. https://doi.org/10.1029/2011JA017139

**Table 1** . Spectral slopes in three regions of near-Earth space for the considered events .

| No. | Date, time | Type, No. of interval | Struc-tures | MHD slope | | | Kinet. slope | | |
|---|---|---|---|---|---|---|---|---|---|
| | | | | SW | Day. MSL | Flank | SW | Day. MSL | Flank |
| 1 | 09.07.14, 17:48 UT | *Slow* , 1 | + | -1.7±0.2 | -1.0±0.3 | – | -2.7±0.1 | -2.6±0.1 | -2.1±0.3 |
| 2 | 09.07.14, 18:13 UT | *Slow* , 2 | – | -1.8±0.2 | – | – | -2.3±0.1 | -2.0±0.1 | -1.7±0.2 |
| 3 | 09.07.14, 18:40 UT | *Slow* , 3 | + | -1.6±0.1 | -1.2±0.3 | -0.8±0.1 | -2.3±0.1 | -2.3±0.1 | -2.4±0.2 |
| 4 | 07.02.14, 17:18 UT | *Sheath* , 1 | + | -1.8±0.1 | -2±0.3 | -1.6±0.1 | -2.5±0.1 | -3.5±0.1 | -3.0±0.1 |
| 5 | 07.02.14, 18:45 UT | *Sheath* , 2 | – | -1.6±0.2 | -0.6±0.2 | -1.5±0.1 | -3.2±0.1 | -3.5±0.2 | -2.8±0.1 |
| 6 | 07.02.14, 22:14 UT | *Sheath* , 3 | + | -1.9±0.1 | -0.5±0.2 | -1.6±0.1 | -4.2±0.2 | -3.0±0.2 | -2.0±0.1 |
| 7 | 08.02.14, 00:40 | *Sheath* , 4 | – | -1.9±0.1 | – | -1.7±0.1 | -3.5±0.2 | -3.2±0.2 | -2.2±0.1 |
| 8 | 16.02.14, 04:08 UT | *Sheath* , 1 | – | -1.8±0.1 | – | -1.4±0.1 | -2.6±0.2 | -3.0±0.2 | -3.2±0.2 |
| 9 | 16.02.14, 04:22 UT | *Sheath* , 2 | + | -1.6±0.1 | – | -1.7±0.1 | -2.9±0.2 | -3.4±0.2 | -2.6±0.2 |
| 10 | 16.02.14, 05:06 UT | MC, 3 | – | -1.9±0.2 | – | -1.7±0.1 | -2.3±0.1 | -4.1±0.2 | -2.8±0.1 |
| 11 | 16.02.14, 05:35 UT | MC, 4 | + | -1.8±0.2 | – | -1.3±0.1 | -2.2±0.1 | -4.8±0.3 | -2.6±0.1 |

Figure captions

**Fig. 1.** ( *a* ) - Ion flux in the SW (dark gray line), in the daytime MSL (light gray line), and on the flank (black line) for the event of July 9, 2014; ( *b, c* ) - measurements of the modulus and components of the magnetic field on THEMIS and Wind satellites, respectively, data from all satellites are shifted by plasma propagation time; ( *d* ) - satellite positions for the event under consideration.

**Fig. 2.** Comparison of normalized spectra of magnetic field modulus (|B|) and ion flux (|F|) fluctuations in three regions of near-Earth space - in the SW (dark gray line), in the daytime MSL (light gray line) and on the flanks (black line) - for the three intervals marked in Fig. 1.

**Fig. 3.** Similar to Fig. 1 for the event of February 7-8, 2014, relating to the compression region *Sheath* .

**Fig. 4.** Similar to Fig. 1 for the event of February 16, 2014, related to ICME with a compression region *Sheath* ahead of it.

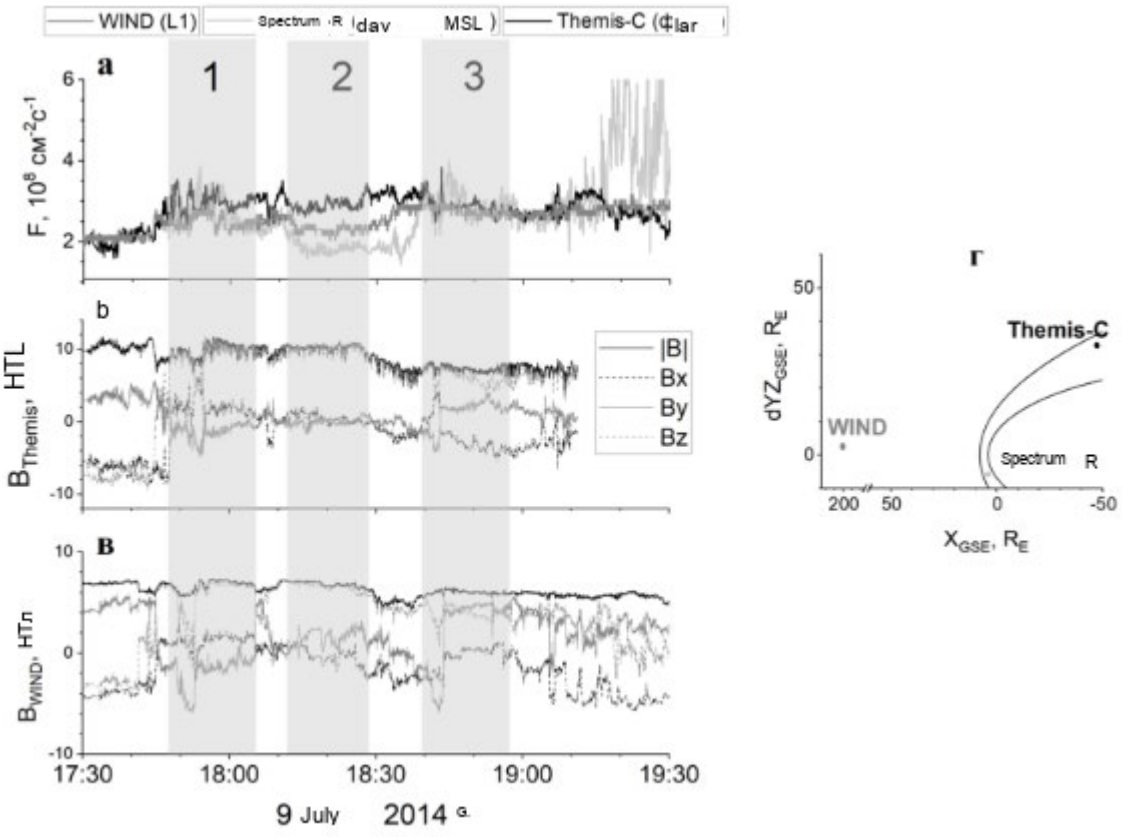
WIND (L1)
Spectrum R
MSL )
Themis-C (
a
1
2
3
F, 10^8 см^-2с^-1
b
|B|
Bx
By
Bz
B_Themis, HTL
B
B_WIND, HTn
17:30
18:00
18:30
19:00
19:30
9 July 2014
г
dYZ_GSE, R_E
Themis-C
WIND
Spectrum R
X_GSE, R_E

Fig. 1.

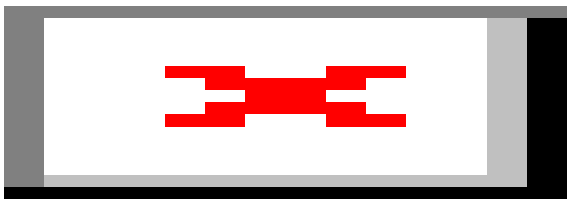

Fig. 2.

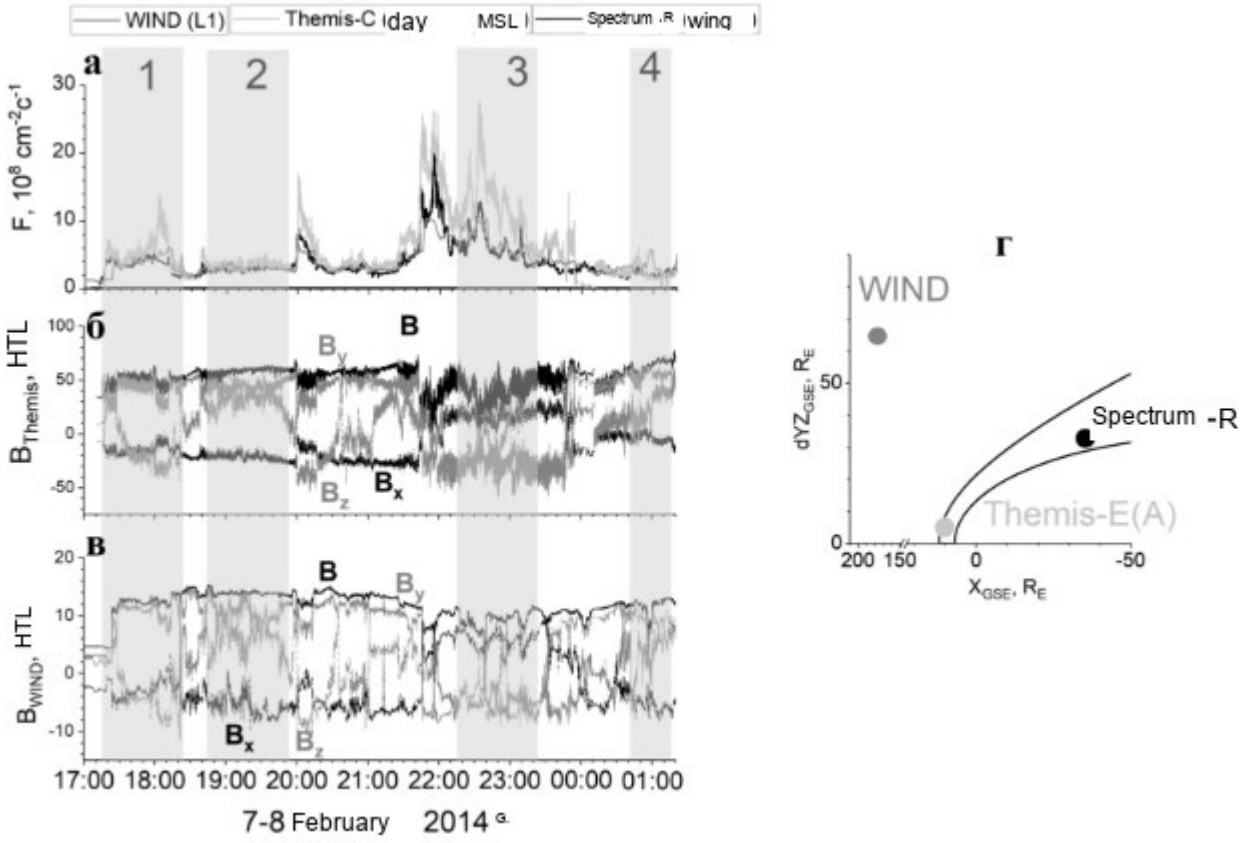
WIND (L1)
Themis-C
MSL
Spectrum -R
а
1
2
3
4
F, 10^8 cm^-2c^-1
б
B
B_Y
B_Z
B_X
B_Themis, HTL
в
B_WIND, HTL
17:00 18:00 19:00 20:00 21:00 22:00 23:00 00:00 01:00
7-8 February 2014 G.
г
WIND
Spectrum -R
Themis-E(A)
dYZ_GSE, R_E
X_GSE, R_E

Fig. 3.

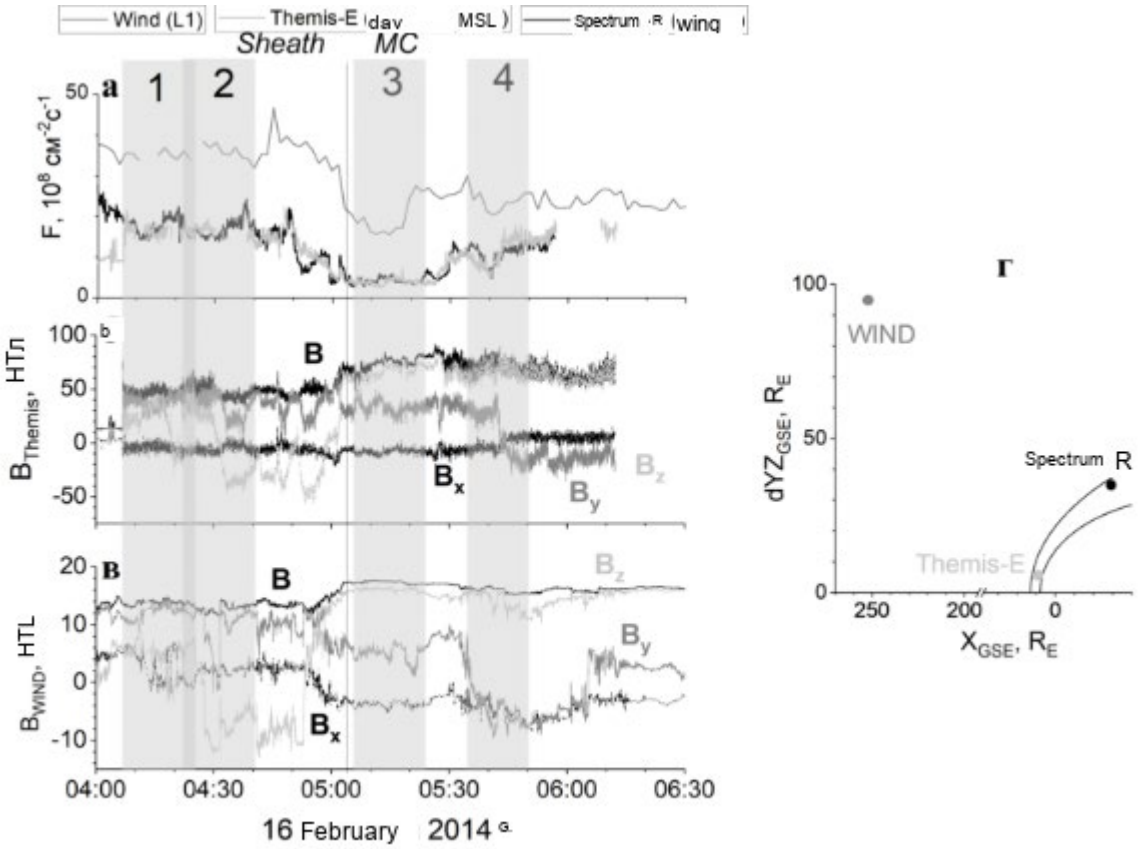
Wind (L1)
Themis-E
MSL
Spectrum
Sheath
MC
1
2
3
4
a
F, 10^6 см^-2с^-1
b
B_Themis, HTn
B
B_x
B_y
B_z
B_WIND, HTL
04:00
04:30
05:00
05:30
06:00
06:30
16 February 2014 г.
г
dYZ_GSE, R_E
X_GSE, R_E
WIND
Spectrum R
Themis-E
250
200
0

Fig. 4.